JOURNAL OF MATERIALS SCIENCE 10 (1975) 1037–1048

Apparent interfacial failure in mixed-mode adhesive fracture

WILLARD D. BASCOM, CARTER O. TIMMONS, ROBERT L. JONES
Surface Chemistry Branch, Naval Research Laboratory, Washington D.C., USA

Aluminium-epoxy adhesive specimens constructed with the bond at 45° to the direction of loading appear to fail very close to the interface. The actual locus of failure was investigated by ^{14}C labelling of the epoxy polymer and also by Auger spectroscopy profile analysis. Both techniques indicated a residual film of polymer a few hundred angstroms thick on the aluminium surface. The fracture energy of these specimens was determined and found to be affected by the surface roughness of the aluminium. The mixed-mode fracture energy ($\mathcal{G}_{(I,II)C}^{45°}$) of these specimens in the absence of any surface roughness effect (polished surfaces) was 140 J m^{-2} compared to 136 J m^{-2} for the same polymer in simple opening-mode $\mathcal{G}_{IC}$ adhesive fracture. The "interfacial" failure and the effect of surface finish on fracture are discussed in terms of the applied stress directing the failure toward the interface but the approach of the crack to the boundary being limited by the size of the crack tip deformation zone.

1. Introduction

The question of whether an adhesive joint can fail at the adhesive-adherend interface has been the subject of intense debate. Bikerman [1] has maintained that if the joint has been properly made with intimate contact between the two phases, an interfacial failure is impossible. Objections have been raised that Bikerman's argument ignores a number of factors that could weaken the interface relative to both phases or that certain unique combinations of material properties of the adjoining phases could result in interfacial crack propagation being favoured.

Nevertheless, Bikerman's generalization has led to the empirical rule that if a bond fails interfacially it had been improperly made because of surface contamination, air entrapment, or other development of a weak boundary layer. Recently, Bikerman [2] has noted that for certain microscopy-replication techniques, failure may occur within a few hundred angstroms of the interface. Although this would still not be true interfacial failure it is apparent, as with other types of bonds that fail "interfacially", that the distinction is very often difficult to make.

Trantina [3] has reported an apparent interfacial failure in what he referred to as a "scarf" joint or, more properly, a combined-mode adhesive fracture specimen. The test configuration (Fig. 1) consisted essentially of two aluminium plates bonded with an epoxy resin and with the bond at angles of from 30 to 90° to the direction of loading. The combined-mode designation

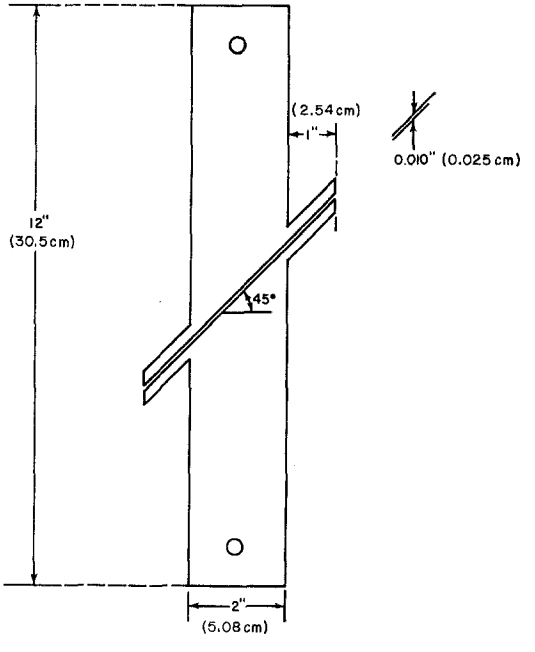

Figure 1 Combined-mode adhesive joint specimen. Plate thickness = 1.3 cm.

arises because fracture involves both cleavage (mode I) and in-plane shear (mode II). He observed that bond failure was apparently interfacial in that the crack always propagated at or very close to the aluminium surface. This was somewhat surprising since joints consisting of the same metal and epoxy resin with the bond at 90° to the loading direction had always exhibited centre-of-bond failure, i.e. layers of resin of approximately equal thickness were evident on both sides of the bond after fracture.

Further work with the Trantina specimen seemed appropriate, mostly to establish the exact locus of failure and to what extent surface parameters (such as surface roughness) affect the failure. Our effort was greatly aided by the fact that Trantina [4] had developed a finite element analysis for the specimen compliance versus crack length, dC/da, so that adhesive strain energy release rates, $\mathcal{G}_{I,II}$, could be computed.

2. Experimental

The epoxy polymer adhesive was the diglycidyl ether of bisphenol A (DGEBA, Dow Chemical Co, DER-332, epoxy equiv. = 175 ± 3) cured with hexahydrophthalic anhydride (HHPA, practical grade, Eastman Organic Chemicals) using benzyldimethylamine (BDMA, 98% Eastman Organic Chemicals) as a catalyst. The anhydride and epoxy were mixed in the ratio of 0.45:1 to which was added 0.2 wt % catalyst. The curing temperature schedule was 2 h at 90°C, 16 h at 120°C and 2 h at 150°C. Pertinent physical properties are listed in Table I. The test methods are described in [5].

TABLE I Physical properties of the HHPA-DGEBA polymer (25°C, 0.13 cm min^{-1})

Tensile strength, σ	4.6 MN m^{-2}
Tensile modulus, E	3.86 × 10^3 MN m^{-2}
Glass transition temperature, T_g	317 K
Opening-mode fracture energy, $\mathcal{G}_{IC}$	136.0 J m^{-2}

Phthalic-7-^{14}C anhydride, used to radioactively label the epoxy polymer, was obtained from International Chemical and Nuclear Corporation. Considering the similarity in the chemical structure of HHPA and ^{14}C phthalic anhydride, it was assumed that the label was uniformly incorporated into the resin structure. A stock solution of the anhydride was prepared by dissolving 8.4 mg (1.0 mCi) of this material in 1 litre of tetrahydrofuran. The adhesive was prepared in 50 g portions and consisted of 34.4 g Dow DER-332, 15.6 g hexahydrophthalic anhydride, 0.1 g benzyldimethylamine and 16.8 × 10^{-4} g of the ^{14}C phthalic anhydride. (This small amount of labelled anhydride was introduced by evaporating 200 ml of the stock solution in the mixing vessel before the addition of the other components.)

Standard samples of known thicknesses, approximating those expected on the fracture samples, were prepared by taking known weights of the labelled adhesive and diluting with tetrahydrofuran. Individual aliquots were then delivered into 1 in. diameter aluminium planchets and the solvent allowed to evaporate before curing the resin. The thicknesses of the standard samples could then be calculated taking the density of the adhesive to be 1.1 g cm^{-3}.

Both the fracture samples and the standard samples were counted with a Nuclear-Chicago Model D-47 gas flow detector operated in the Geiger region. The counting efficiency was about 30% for the 0.155 MeV β of ^{14}C. A calibration curve of activity versus thickness is given in Fig. 2.

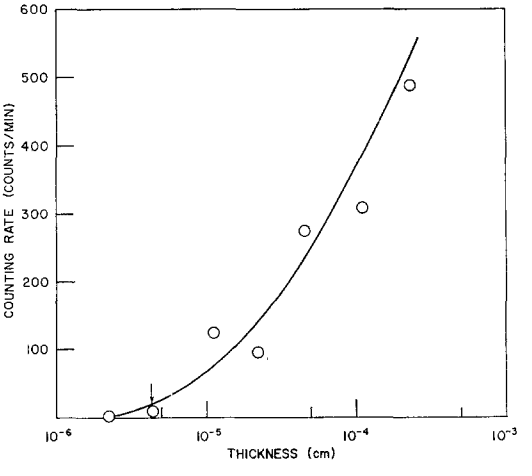

Figure 2 Film thickness versus counting rate calibration curve.

The aluminium adherends were cut and machined from nominally 0.5 in. (1.3 cm) plates of 2024 or 6061 aluminium alloys to the dimensions given in Fig. 1. Work was restricted to 45° bond angle specimens since Trantina had found that at this bond angle the crack had the least tendency to jump from one interface to the

other. Our specimens differed from his in that we used two side arms instead of one. This modification made it easier to position and clamp the two plates.

To study the effect of surface finish on joint strength, the adherends were either milled with a high speed cutter, abraded with a 600 grit or 180 grit paper, or polished to a mirror surface with an Al_2O_3-water slurry on a metallographic wheel. The milled and abraded surfaces were further cleaned by an acid-chromate etch followed by rinsing in tapwater. The polished surfaces were not etched. Surface roughness was measured using a Talysurf-4 profilometer (Rank Precision Industries, Ltd).

The specimens were assembled with 0.025 cm Teflon spacers between the side arms to establish the bond thickness. The arms were clamped with spring clips. One side of the bond was sealed with a high-temperature, pressure sensitive tape and the liquid epoxy mixture was fed into the resulting slit. Contamination of the epoxy by the tape adhesive was prevented by interposing a narrow strip of Teflon coated aluminium foil.

After the epoxy was cured, the tape, foil and any exuded resin were abraded away with a wire brush. A sharp precrack was introduced by carefully wedging open the side arms. The specimen was then pulled in tension to failure using the model TT-B Instron at a strain rate of 0.13 cm min^{-1} and at 25 $\pm$ 2°C.

Post-failure examinations of the failed specimens were made by cutting sections approximately 2.5 cm $\times$ 0.5 cm from the adhesive and adherend sides of the bond. The sections were examined by scanning electron microscopy (SEM, Advanced Metal Research Model 1000) and Auger spectroscopy (Physical Electronics Industries Model 50-220). Radiation counting was also done on specimen surfaces of this size but masked down to an area of 1.80 cm^2.

The combined mode fracture energies, $\mathcal{G}_{(I,II)C}{}^{45°}$, were computed from the finite element analysis of Trantina [4]. The *total* stress intensity parameter values taken from [4] are listed in Table II. The $K_{I,IIC}$ at the failure load, P_C, was calculated from this calibration and then converted to the fracture energy (strain energy release rate) $\mathcal{G}_{(I,II)C}{}^{45°}$ by,

$$(K_{(I,II)C}{}^{45°})^2 = (\mathcal{G}_{(I,II)C}{}^{45°})E \qquad (1)$$

where E is the tensile modulus of the aluminium adherends, taken here as 7.24 $\times$ 10^4 MN m^{-2} (10.5 $\times$ 10^6 psi)*.

TABLE II Total stress intensity parameter 45° bond angle [4]

a/w	$\frac{KB\sqrt{w}}{P}$	a/w	$\frac{KB\sqrt{w}}{P}$
0.07	0.33	0.37	1.17
0.11	0.47	0.46	1.50
0.16	0.61	0.56	1.96
0.22	0.75	0.67	2.50
0.29	0.93		

a = crack length, w = specimen width (5.1 cm), B = specimen thickness (1.3 cm), P = tensile load, K = stress intensity factor.

The opening-mode ($\mathcal{G}_{IC}$) bulk and adhesive fracture behaviour of this DGEBA-HHPA epoxy resin was also examined using the methods described in [5].

3. Results

The fracture energies, $\mathcal{G}_{(I,II)C}$ and the residual film thicknesses, h_r, on the adherends are listed in Table III for test specimens having different surface finishes. Every specimen exhibited an apparent interfacial failure. However, the fracture energy and the locus of failure (i.e., the residual film thickness) appear to be a function of surface finish although they did not correlate in any simple manner with the centre-line-average (CLA) roughness.

Profilometer traces of the four different surface finishes are presented in Fig. 3. Note that the vertical magnifications are different. A point of some importance in this figure is that although the CLA values of the milled surface and the 180 grit abraded surface were nearly equal, the distance between asperities of the latter was much smaller. In fact, the asperitie distance was relatively close for both of the abraded surfaces.

Scanning electron micrographs of the four surface finishes and of the corresponding fracture surfaces are presented in Figs. 4 to 7. The following features should be noted: (a) the adhesive surface gave a detailed replication of the roughness when fractured from the milled and the abraded surfaces. This replication was most evident at the lower magnification; (b) at the higher magnification there is clear indication of a fine detail in the fracture surfaces that was not present on the original adherend. This detail

*10^3 psi = 6·89 N mm^{-2}

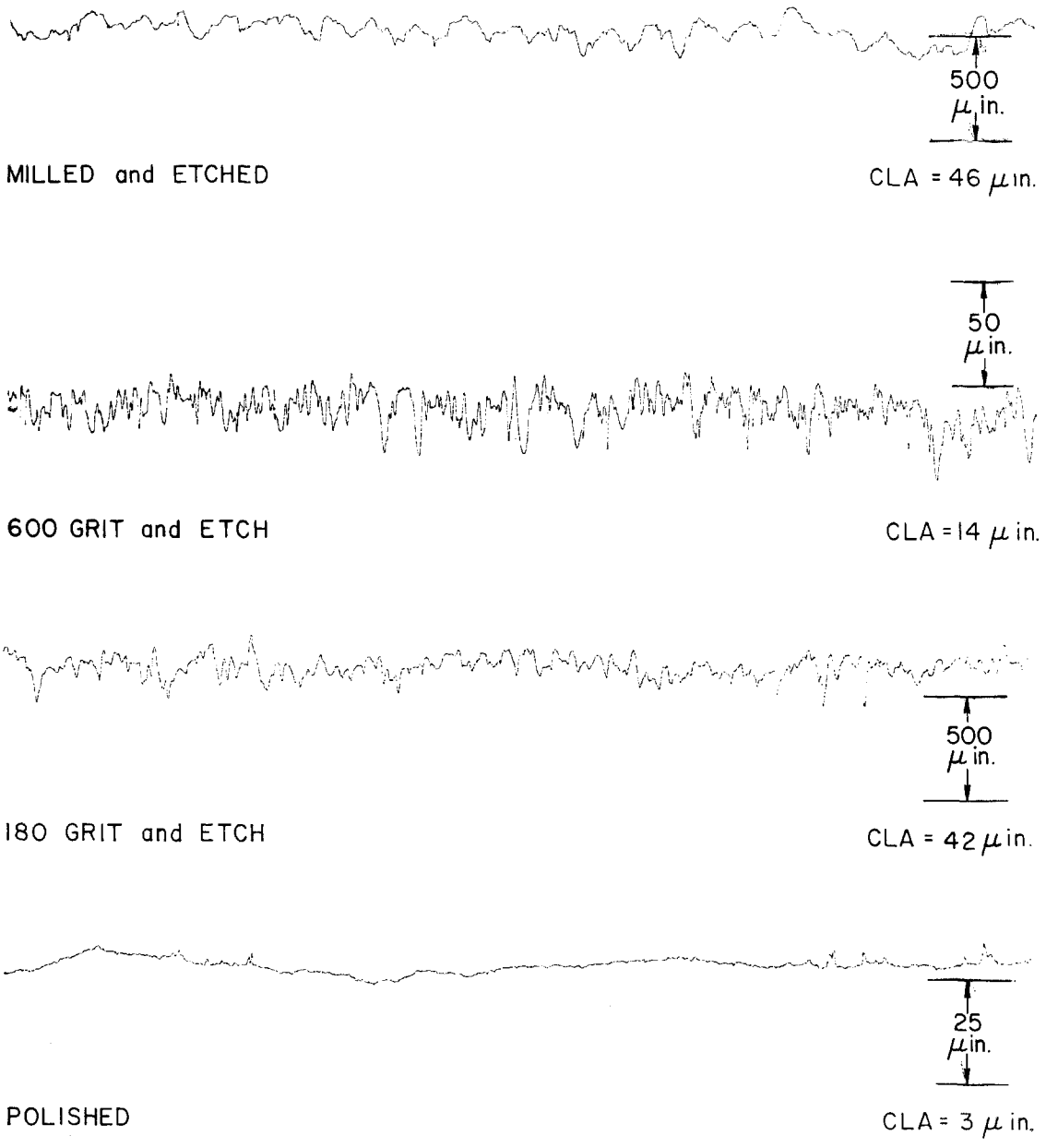

Figure 3 Profilometer traces of the various surface finishes. Each trace represents a traverse of 25.4 cm (1 μin. = 0.025 μm).

is evident on the fractures from the milled specimens as a network of cusps (Fig. 4); (c) the fractures from polished surfaces exhibited parabolic markings (Fig. 7), which are raised above the fracture plane on the adherend side of the fracture and are indentations in the adhesive side. Note the foci within the parabolas and the deformation lines radiating from the foci. The direction of crack propagation was toward the open end of the parabolas.

Polished adherend surfaces were examined using Auger spectroscopy. Profiles of surface composition were obtained by successive argon ion sputtering and analysis. In Fig. 8 a compari-

son is given of the profile analyses of a polished surface that had not been bonded and one that had a residual film of adhesive. Both surfaces gave a carbon signal as well as the expected oxygen and aluminium signals. However, the carbon signal from the post-failure surface was stronger and more persistent. Also, there was a delay in the appearance of the aluminium signal compared to the "clean" surface. If we assume a reasonable sputtering rate of 2 Å min^{-1} for carbon, the carbon profile for the residual film had decreased significantly after removal of 100 Å. This is considerably less than the 640 Å thickness obtained for this film by radioactive labelling (Table III). SEM examination of the surface after the ion sputtering analysis revealed that the parabolic markings had not been removed but only rounded off. Evidently, the decline in the carbon signal represents the removal of the thinner regions of film between the parabolas whereas the radiotracer estimate is an average thickness.

4. Discussion

The apparent interfacial failure of these mixed-mode adhesive specimens is best described as a mechanical focusing of the failure into the interfacial region. The schematic drawing in Fig. 9 illustrates this point. The precrack $\overline{AB}$ is formed by wedging open the side arms. Sub-

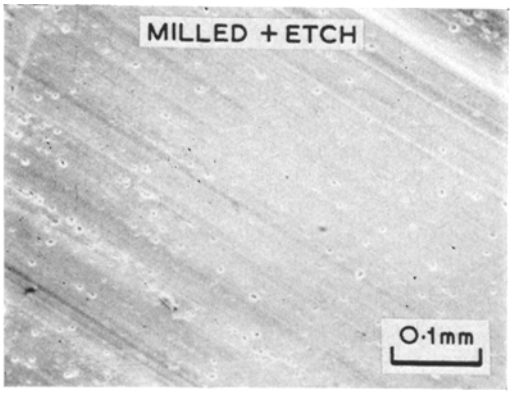

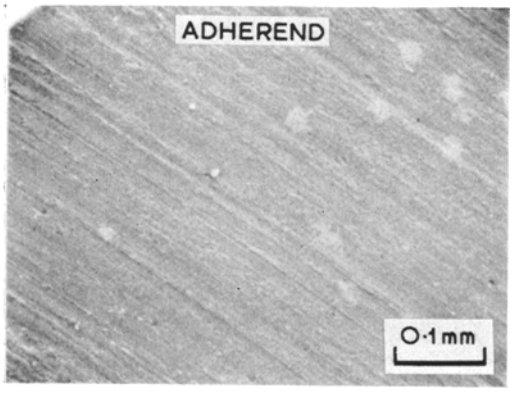

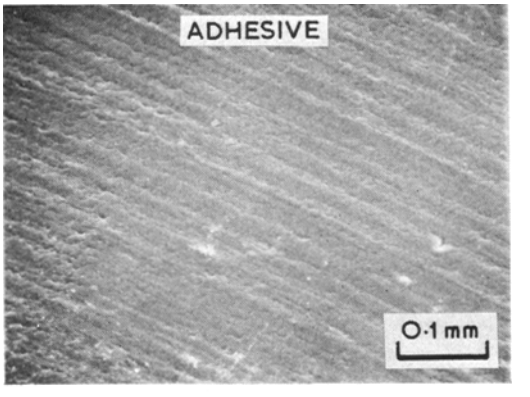

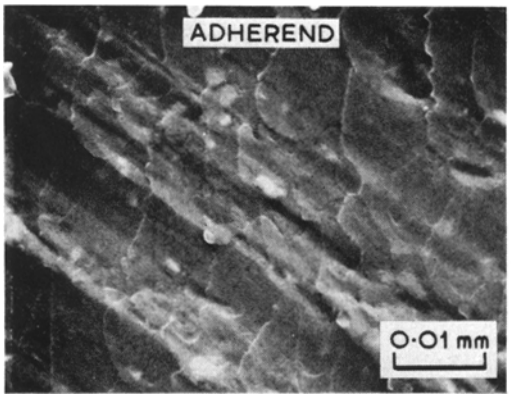

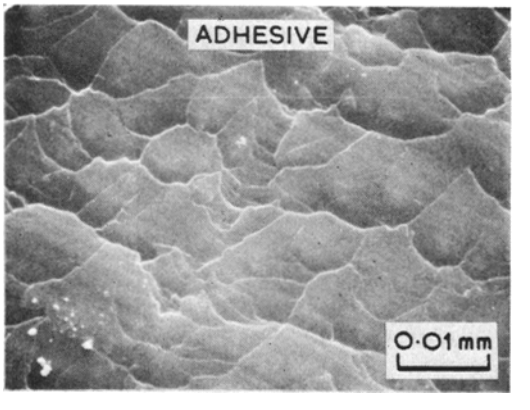

Figure 4 SEM photographs of the milled surface before bonding (top) and the adherend and adhesive surfaces after fracture.

sequent loading of the specimen in tension propagates the crack at 90° to the loading direction along $\overline{BC}$, just as if it were in an isotropic material. There is ample evidence, both theoretical [6, 7] and experimental [7-9], that opening-mode failure is the preferred fracture mode in isotropic polymers and metals. However, the crack $\overline{BC}$ cannot proceed into the aluminium adherend because of the much higher fracture toughness of the metal. Consequently, the crack arrests until the load on the specimen is increased sufficiently to allow propagation parallel to the interface, i.e. along $\overline{CD}$.

A point of some importance is that even though the crack is directed toward the interface along $\overline{BC}$, the approach of the crack to the metal is limited by the zone of deformation at the crack tip. An estimate of the spherical radius, r_y, of this zone for an elastic-plastic material [10] is given by

$$r_y = \frac{1}{6\pi} \frac{E\mathcal{G}_{IC}}{\sigma_{y^2}} \tag{2}$$

and using measured values (Table I) of the tensile modulus, E, tensile strength, σ_y, and opening-mode fracture energy, $\mathcal{G}_{IC}$, a zone radius of about 4×10^{-4} cm is obtained for the HHPA-DGEBA polymer. For a crack tip near the metal/polymer boundary, the deformation zone will lay predominantly within the lower

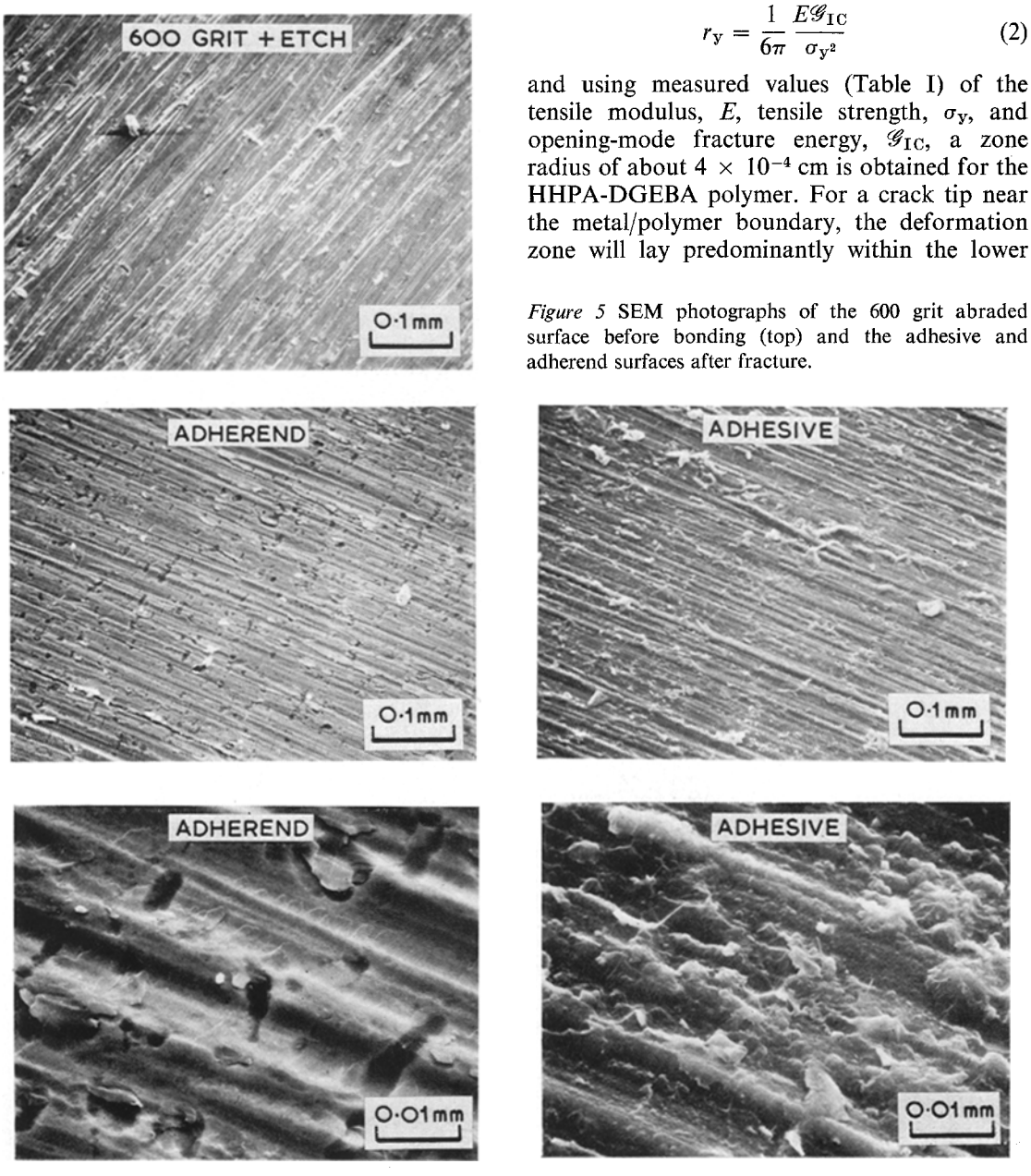

Figure 5 SEM photographs of the 600 grit abraded surface before bonding (top) and the adhesive and adherend surfaces after fracture.

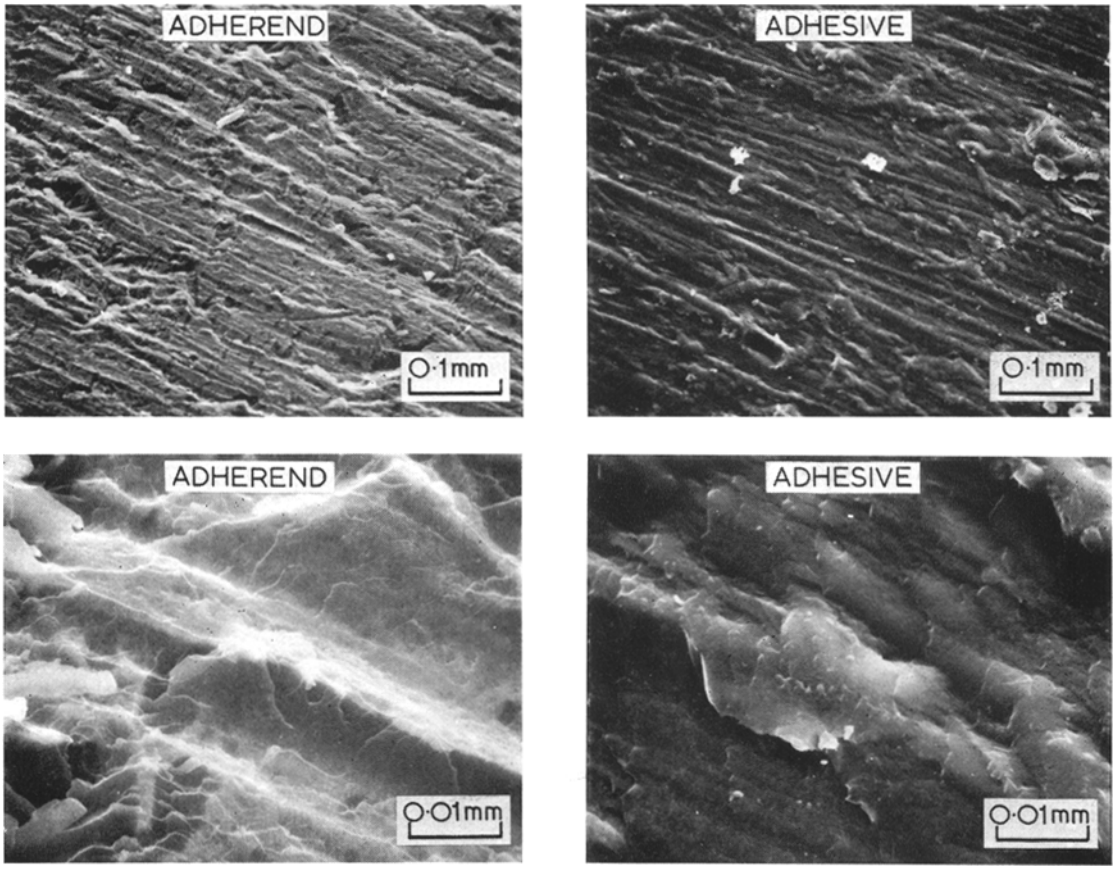

Figure 6 SEM photographs of the adhesive and adherend fracture surfaces from the 180 grit abraded specimens.

modulus polymer rather than in the much higher modulus metal since the elastic modulus is an inverse function of energy storage at a given stress. Since cracking occurs within the centre of this zone, the locus of failure will parallel the interface but in the polymer at a distance of approximately r_y from the metal.

Equation 2 does not take into account the mixed-mode stress distribution that exists at the crack tip at point C (Fig. 9). A more exact expression can be obtained from Pook [8]

$$r_{y(I,II)C} \approx \frac{1}{6\pi\sigma_{y^2}} E(\mathscr{G}_{IC} + 3\mathscr{G}_{IIC}) . \quad (3)$$

Since $\mathscr{G}_{IC} \approx \mathscr{G}_{IIC}$ then $r_{y(I,II)C} \approx 4r_{yC}$, i.e. Equation 2 may underestimate the zone size by a factor of four.

Actually, failure occurred much closer to the interface than would be expected from these fracture mechanics considerations. The residual film thickness listed in Table III for the milled and abraded surfaces must be corrected for

TABLE III Effect of roughness on combined-mode failure

Surface treatment	Roughness* (μm)	h_r (Å)	$\mathscr{G}_{(I,II)C}^{45°}$ (J m^{-2})
Milled + etched	1.17	2150	290 ± 90
180 grit + etch	1.07	8950	123 ± 27
600 grit + etch	0.36	2600	82 ± 33
Polished	0.08	640	140 ± 63

*Centre-line-average (CLA).

surface roughness since the ^{14}C measurements are based on a nominal surface area. In the case of the 600 grit abraded surfaces the roughness factor [11] was approximately 4 and applying this correction gives a film thickness of 650 Å assuming the crack followed the roughness exactly. The measured film on the polished surfaces, 600 to 700 Å, does not require a roughness correction. Clearly, these film averages are lower by a factor of ten than even Equation 2 would predict.

There are at least two possible reasons for this discrepancy between predicted and measured residual film thickness. First, the films were measured in regions of fast crack propagation whereas Equations 2 and 3 are for crack initiations. Assuming a proportionality between r_y and the $\mathcal{G}$ of a moving crack it would require the latter to be near the ideal brittle limit of 0.5 J m^{-2} in order to account for film < 500 Å. Second, it is possible that the development of the deformation zone is in some way restricted for a crack tip near an interface. This may in fact be the case since there was far less evidence (SEM) of polymer deformation in the region of initiation of these mixed-mode adhesive specimen than in bulk $\mathcal{G}_{IC}$ tests of the same polymers or $\mathcal{G}_{IC}$ adhesive tests where the crack went centre-of-bond.

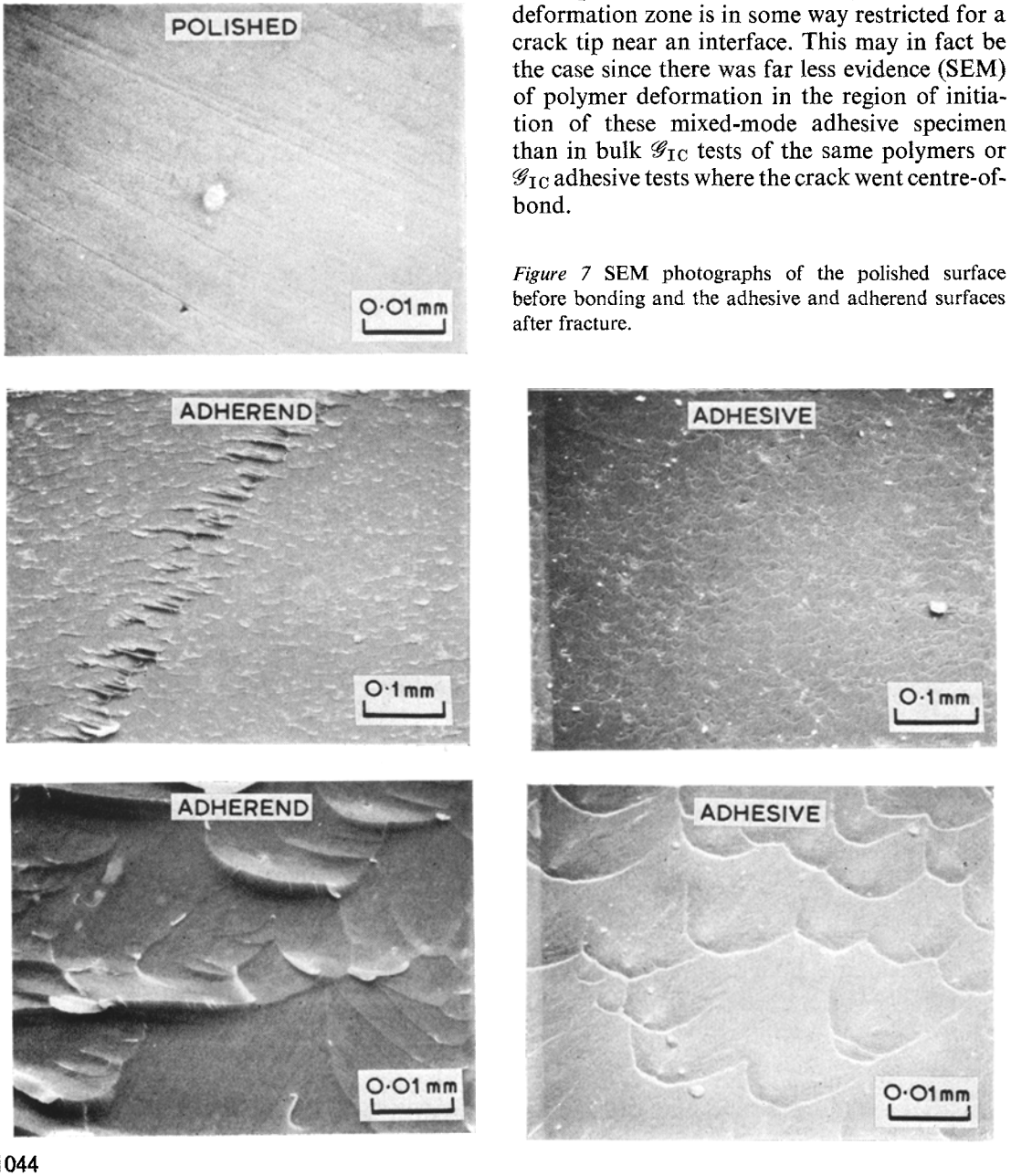

Figure 7 SEM photographs of the polished surface before bonding and the adhesive and adherend surfaces after fracture.

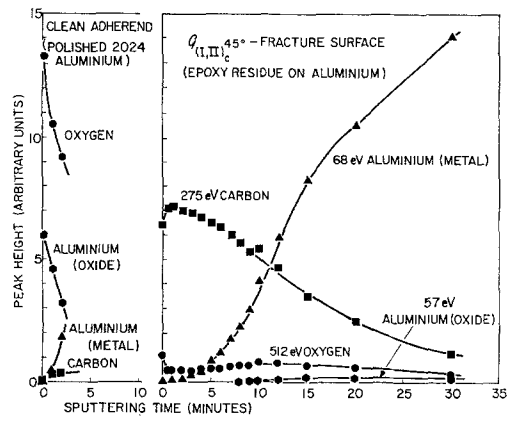

Figure 8 Auger spectroscopy profiles of a polished surface before bonding and the adherend side after fracture. The peak height units were equal for the same element on both surfaces but were not necessarily equal for different elements.

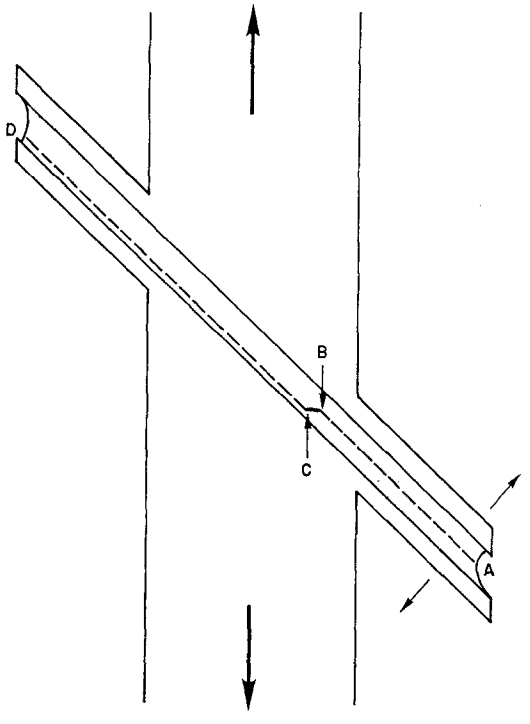

Figure 9 Schematic representation of the "focusing" of a centre-of-bond precrack toward the interface.

Another possible reason for such thin residual films is that failure occurs in a plane determined by the molecular configuration of the polymer near the interface or by residual thermal stresses that develop during the resin cure. However, this explanation is difficult to reconcile with the fact that the same epoxy exhibits a clearly centre-of-bond failure in mode I specimens. The adherend pretreatment and the cure schedule were identical in both cases. If the interfacial region were inherently weak then opening mode specimens would also be expected to exhibit an apparent interfacial failure.

The effect of surface roughness on the fracture energy was complex. The results suggest two opposite effects. In the first case, if the spacing between asperities is large enough that the crack tip can enter the groove between them, then in order to "pull" the crack out, energy is needed over that required to initiate a crack along a planar surface. This appears to be the situation for the milled surface for which $\mathcal{G}_{(I,II)C}{}^{45°}$ was nearly twice that for the polished surface. (In the latter case the scratches were not replicated and so evidently too shallow to affect crack initiation.)

The abraded roughness had the effect of lowering the fracture energy compared to the value for polished surfaces. Part of the reason was that the distance between asperities was too small to allow crack penetration. Consistent with this explanation is the fact that the failure occurred much further from the interface on the 180 grit surface than on the milled surface even though the CLA roughness values were nearly equal. However, some other factor must have also affected fracture from the abraded surfaces to lower the energies below that of the polished specimen. Quite possibly the very sharp, closely spaced asperities act as points of stress concentration and thereby enhance the strain energy in the crack tip deformation zone during initiation and as the crack propagated.

In a study of adhesive butt-joint specimens, Jennings [12] found polished adherends to give lower joint strength than sandblasted specimens. For DGEBA-polyamide epoxy between aluminium bars the difference in tensile strength was a factor of about two which translates to a fracture energy difference of X4 (assuming comparable initiation flaw sizes). Failure of these butt joints was described as usually starting at the bond perimeter near the interface and so would appear to be a mixed-mode fracture since there are both tensile and shear forces acting in this region. Jennings also determined butt-joint strengths using abraded aluminium surfaces but unlike the results here found them to be essen-

tially the same or slightly higher than when the adherends were polished.

Mulville [13] has studied the effect of surface roughness on the fracture energy of specimens consisting of an epoxy plate cast onto an aluminium plate (the polymer was DGEBA cured with tetraethylenepentamine). Failure was induced along the epoxy-aluminium boundary by tensile loading of the aluminium parallel to the bond. This produced a combination of shear and tensile forces at the crack tip which produced a mixed-mode, interfacially directed failure. The surface topography of the aluminium was replicated by the epoxy but there was visible evidence of a thin polymer layer on the adherend. Mulville found a systematic increase in $\mathcal{G}_C$ with surface roughness for polished, milled, glass peened and sand blasted surfaces. The values for polished (no etch) and milled adherends differed by about a factor of two just as was observed here.

Turning now to the fine-scale fracture mark ings on the various failed surfaces, it would appear that micro-cracking had occurred ahead of the main crack front. The parabolic markings on the surfaces fractured from polished adherends (Fig. 7) are quite characteristic of advance micro-cracking [14] and are generally attributed to the crack front passing through microcracks growing radially in a plane that is tilted with respect to the plane of the main crack. Quite probably the microcracks are the result of dilatational ($\mathcal{G}_I$) failure at points of weakness in the resin ahead of the main crack front which advances by shear failure parallel to the interface. This process is illustrated schematically in Fig. 10. A similar, albeit more complex, microfracture occurred with the milled adherends and gave rise to the network of cusp-like features in Fig. 4. These fine-scale fracture markings were not observed on the fracture surfaces of these epoxy resin in pure opening-mode failure.

In Table IV, a comparison is made of the opening-mode adhesive fracture energy $\mathcal{G}_{IC}$ of this anhydride-epoxy with the $\mathcal{G}_{(I,II)C^{45°}}$ obtained using polished adherends (for which the adherend roughness effect was minimal). The mixed-mode energy was somewhat higher than the opening-mode energy, as is generally found for the fracture of isotropic materials [7, 9]. Indeed, this is the basis for expecting crack propagation to occur perpendicular to the direction of tensile loading. Mulville [13] found the $\mathcal{G}_C$ for his bonded epoxy-aluminium plate

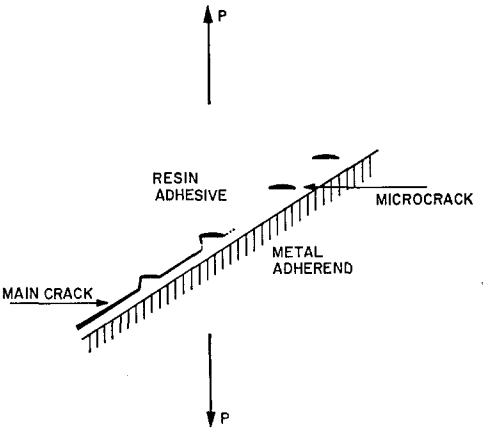

Figure 10 Schematic of microcrack formation and intersection with main crack front.

TABLE IV Fracture energies of the HHPA-DGEBA polymer

	$\mathcal{G}_{IC}$ (J m^{-2})		$\mathcal{G}_{(I,II)C}$ (J m^{-2})
	This work	[24]	
Adhesive	116	121	140
Bulk	136		

specimen (polished adherends) to be 70 J m^{-2} which was approximately equal to the $\mathcal{G}_{IC}$ value reported by Mostovoy [15] for the same DGEBA-amine cured material. Trantina [3], in his study of the scarf-joint specimen with various bond angles observed an increase in fracture energy as the mode II contribution was increased. Very likely this trend was real although the magnitude of the mixed-mode energies was probably high due to a surface roughness effect since his adherend surfaces had been milled and etched.

A note of caution must be made that although the relative magnitude of the adhesive $\mathcal{G}_I$ and $\mathcal{G}_{I,II}$ was consistent with isotropic materials in this study and in the work of Mulville and Trantina, a very different result is being found for elastomer-modified epoxies and commercial structural adhesives [16] which exhibit mixed-mode adhesive fracture energies that are an order of magnitude less than the corresponding opening-mode adhesive energies.

Interfacial failure. The locus of failure of the scarf joint specimens studied here was in the adhesive resin but less than 1000 Å from the interface. This near interfacial failure was judged to be the result of the stresses directing

the failure into the interfacial region. If this explanation is correct, then apparent interfacial failures of this type are to be expected for many adhesive joint designs when the loading results in both tensile and shear stresses acting in the bond.

Indeed, the work by Jennings [12] with butt-joints in tension and by Mulville [13] whose specimen was essentially a butt joint loaded in shear appear to be instances of interfacially focused failure resulting from the presence of tensile and shear components acting at the crack tip. There is also the work by Wilcox and Jemian [17] who report an apparent interfacial failure of thick-bond, lap-shear specimens which they attribute to the fracture being mechanically directed into the interfacial region. They also noted that although the locus of failure was near the interface there was a thin residual film left on the metal.

Still another example is the interfacial-cohesive failure transition observed in the peel adhesion of pressure sensitive tapes from rigid substrates [18]. At low strain rates there is a general yielding of the entire adhesive interlayer between the tape and substrate. As the peel rate is increased the region of viscoelastic (and viscoplastic) deformation is reduced and tends to be restricted to the interfacial region. Since there are both tensile and shear forces acting at the peel front even at a 90° peel angle [19] it seems reasonable that at the high strain rates failure is being focused into the interfacial region in the sense discussed here. Indeed, Hunstberger [20] has made this same point in discussing the locus of failure in peel adhesion. The apparent interfacial failure that Bikerman noted in connection with the stripping of microscopy replicas [2] is very likely a case of "interfacial" peel adhesion. The failure is, nonetheless, cohesive in that a thin film of the replicating polymer is left on the substrate. A similar situation was encountered in some exploratory work [21] with aluminium sheets bonded to the ^{14}C labelled anhydride-epoxy and tested in 90° peel. Failure occurred at about 500 Å from the interface yet the machine markings on the metal had been replicated on the epoxy fracture surface. However, there have been cases reported of interfacial peel that appear to be true adhesion failure (molecular separation along the adhesive/adherend boundary), notably the systems reported by Huntsberger [20, 22] and Kaelble and Reylek [23]. In these instances the strain rate and/or temperature and the chemical constitution of the adhesive and adherend were such that the cohesive rheological response of the adhesive layer was slow compared to the rheological response of the material in immediate contact with the adherend and the thermodynamic work of adhesion was low compared to the work of cohesion of the adhesive. Nonetheless, we would expect that some nonrecoverable work is done on the adhesive in the interfacial region so that the peel energy is not reduced to the ideal limit corresponding to the thermodynamic work of adhesion.

Perhaps the most important point is not whether true interfacial failure can occur but the fact that whenever the stress distribution focuses failure into the interfacial region, the surface properties of the adherend will influence joint strength. In effect, the crack "knows" the interface is there by virtue of the deformation zone that invariably exists at the crack tip. For this reason joint strength will be sensitive to the condition of the adherend surface (notably its roughness) and to any effect the surface might have on the chemical structure, rheological response or environmental sensitivity of the adhesive in the interfacial region.

References

1. J. J. BIKERMAN, "The Science of Adhesive Joints", 2nd Edn. (Academic Press, New York, 1968).
2. J. J. BIKERMAN, *Microscope* **21** (1973) 183.
3. G. G. TRANTINA, *J. Comp. Mat.* **6** (1972) 371.
4. *Idem*, T and AM Report 352, Univ. of Illinois, Urbana (1971).
5. W. D. BASCOM, R. L. COTTINGTON, R. L. JONES and P. PEYSER, *J. Appl. Polymer Sci.* in press.
6. G. R. IRWIN, *Trans. ASME, J. Appl. Mech.* **24** (1957) 361.
7. F. ERDOGAN and G. C. SIH, *Trans. ASME, J. Basic Eng.* **85** (1963) 519.
8. L. P. POOK, *Fracture Mech.* **3** (1971) 205.
9. J. G. WILLIAMS and P. D. EWING, *Int. J. Fracture Mech.* **8** (1972) 441.
10. J. R. RICE, in "Fracture, An Advance Treatise", Vol. II, edited by H. LIEBOWITZ (Academic Press, New York, 1968) p. 191.
11. C. O. TIMMONS, R. L. PATTERSON and L. B. LOCKHART, JUN, *J. Colloid and Interface Sci.* **26** (1968) 120.
12. C. W. JENNINGS, in "Recent Advances in Adhesion", edited by L. H. Lee (Gordon and Breach, New York, 1973) p. 469.
13. D. R. MULVILLE and R. H. VAISHNAV, Army Symp. on Solid Mechanics, 10 September 1974, Army Materials and Mechanics Research Center, Watertown, Mass.

14. I. WOLOCK and S. B. NEWMAN, "Fracture Processes in Polymeric Solids" (Interscience, New York, 1964) p. 235.
15. S. MOSTOVOY and E. J. RIPLING, *J. Appl. Polymer Sci.* **15** (1971) 661.
16. W. D. BASCOM and C. O. TIMMONS, work in progress.
17. R. C. WILCOX and W. A. JEMIAN, *Polymer Eng. and Sci.* **13** (1973) 40.
18. D. H. KAELBLE, *Trans. Soc. Rheol.* **15** (1971) 275.
19. D. H. KAELBLE and C. L. HO, *ibid* **18** (1974) 219.
20. J. R. HUNTSBERGER, *J. Polymer Sci.* **1A** (1963) 1339.
21. W. D. BASCOM and R. L. COTTINGTON, unpublished results.
22. J. R. HUNTSBERGER, *J. Polymer Sci.* **1A** (1963) 2241.
23. D. H. KAELBLE and R. S. REYLCK, *J. Ahesion* **1** (1969) 102, 124.
24. E. J. RIPLING, C. BERSCH and S. MOSTOVOY, Proceedings of the 1970 National SAMPE Conference, Vol. 2 (1970) p. 287.

Received 29 August and accepted 11 November 1974.